

Deep sea NMR: Methane hydrate growth habit in porous media and its relationship to hydraulic permeability, deposit accumulation, and submarine slope stability

R. L. Kleinberg, C. Flaum, and D. D. Griffin

Schlumberger-Doll Research, Ridgefield, Connecticut, USA

P. G. Brewer, G. E. Malby, and E. T. Peltzer

Monterey Bay Aquarium Research Institute, Moss Landing, California, USA

J. P. Yesinowski

Naval Research Laboratory, Washington, District of Columbia, USA

Received 3 January 2003; revised 22 May 2003; accepted 2 July 2003; published 29 October 2003.

[1] Review of the literature reveals that the nature of pore-scale interactions between gas hydrates and porous media remains a matter of controversy. To clarify the situation, nuclear magnetic resonance (NMR) measurements have been made on methane hydrate-bearing sandstones. The samples were synthetically prepared within the gas hydrate stability zone, at or near the seafloor in Monterey Bay, California. The method simulated natural hydrate deposition by gas flows that are not in thermodynamic equilibrium with the surrounding earth. The efficiency of hydrate production was variable, as has been observed elsewhere. When substantial hydrate saturations were achieved, NMR relaxation time measurements indicated that hydrate tended to replace water in the largest pore spaces. The relative permeability to water, as determined by an NMR-based correlation, was significantly reduced. The magnitude of this reduction was also consistent with formation of hydrate in the centers of pores, rather than with hydrate coating the grains. The growth habit suggested by these results is consistent with creation of hydrate nodules and lenses in coarse, unconsolidated sediments. It is also consistent with scenarios in which methane gas is delivered efficiently to the atmosphere as a result of seafloor slope failure, thereby strengthening global warming feedback mechanisms. *INDEX TERMS*: 3022 Marine Geology and Geophysics: Marine sediments—processes and transport; 3094 Marine Geology and Geophysics: Instruments and techniques; 5114 Physical Properties of Rocks: Permeability and porosity; 5194 Physical Properties of Rocks: Instruments and techniques; *KEYWORDS*: methane hydrate, pore geometry, growth habit, permeability, seafloor stability, climate change

Citation: Kleinberg, R. L., C. Flaum, D. D. Griffin, P. G. Brewer, G. E. Malby, E. T. Peltzer, and J. P. Yesinowski, Deep sea NMR: Methane hydrate growth habit in porous media and its relationship to hydraulic permeability, deposit accumulation, and submarine slope stability, *J. Geophys. Res.*, 108(B10), 2508, doi:10.1029/2003JB002389, 2003.

1. Introduction

[2] The bulk thermodynamic, transport, and mechanical properties of methane hydrate have been thoroughly investigated. However, within the geophysics community hydrates are of most interest not in bulk form but as constituents of earth formations, either beneath the seafloor or under permafrost. Therefore the relationship between natural gas hydrates and the sediments in which they reside is as important as their bulk properties. This is particularly true because hydrates are generally found in unconsolidated sediments. The thermal conductivity and the speed of sound are affected by pore-scale interactions between hydrate and the host sediment. The mechanical stability of the seafloor

and wellbores in hydrate-affected regions depends crucially on whether hydrate cements mineral grains or merely resides in the pore space between them. Scenarios for the production of natural gas from hydrates depend on how hydrate saturation affects hydraulic permeability, which in turn depends on the pore-space microgeometry.

[3] There are several ways in which hydrate can interact with an unconsolidated packing of mineral grains [Helgerud, 2001]: (1) hydrate forms preferentially at grain contacts, acting as a cement even in small quantities; (2) hydrate coats grains more or less uniformly, progressively cementing them as the hydrate volume increases; (3) hydrate grows in the interior of pores partially supporting the frame; (4) hydrate grows without significant interaction with the frame. Little is known about the controls on growth habit, which could include sediment mineralogy and texture, water salinity, other solutes such as biosurfactants, gas composition, and

whether hydrate forms from free or dissolved gas. Rate and annealing effects may also be factors.

2. Previous Investigations of Pore-Scale Microstructure

2.1. Analogies to Water Ice

[4] There is a large literature on the freezing of ordinary water ice in porous media. It appears to be well established that hydrophilic porous media such as sands and sandstones remain liquid-water-wet in the presence of water ice [Anderson, 1967; Handa *et al.*, 1992; Churaev *et al.*, 1993; Overloop and Van Gerven, 1993; Dash *et al.*, 1995; Valiullin and Furo, 2002]. It can be argued that the growth habits of ice and hydrate are likely to be similar because many of their physical properties are similar [Dvorkin *et al.*, 2000]. Density, Poisson's ratio, and heat capacity are indeed very similar. The elastic moduli of ice are modestly higher than those of Type-I hydrate. Contact angle and surface tension of the liquid water interface appear to be similar for ice and hydrate [Wilder *et al.*, 2001]. On the other hand, the heat of fusion per unit mass is substantially different, and the thermal conductivity of ice is four and a half times larger than that of hydrate [Dvorkin *et al.*, 2000], differences which might influence growth habit.

2.2. Natural Core Recovery

[5] The examination of borehole cores provides insights into hydrate growth habits, but this technique is often not as direct as one might hope. Because natural gas hydrate is not stable at wellhead conditions, hydrate dissociates while core is recovered and transferred to measurement apparatus. Even sophisticated pressure-core recovery techniques [Kvenvolden *et al.*, 1983; Graber *et al.*, 2002] only partially mitigate these problems. Although large nodules and lenses may remain substantially intact in the core barrel, the fate of hydrate disseminated in the pore space of rock and sediment is indeterminate.

[6] Analysis of cores recovered from Blake Ridge [Ginsburg *et al.*, 2000] and the Cascadia margin [Shipboard Scientific Party, 2002] (available on the World Wide Web: http://www-odp.tamu.edu/publications/prelim/204_prel/204PREL.PDF) revealed that hydrates grew preferentially in coarse-grained sediments. This was determined not from direct observation but from measurement of pore water chlorinity anomalies. By the time the core was recovered to the surface, the hydrate had decomposed, leaving relatively fresh water as a marker of its former existence. Core samples from a well in the Canadian Arctic, subjected to extensive analysis [Winters *et al.*, 1999], also revealed that hydrate resided primarily in the coarsest sand and gravel intervals; much less hydrate was found in fine-grained mudstones. Similar trends were noted in borehole cores from the Nankai Trough [Matsumoto, 2002].

2.3. Synthetically Prepared Samples

[7] Sample integrity can be assured in laboratory experiments performed on synthetic samples at controlled temperatures and pressures. However, it is difficult to create methane hydrate in the laboratory under conditions similar to those in nature. Realistic fluxes of dissolved or gaseous methane are difficult to simulate in small laboratory pres-

sure vessels at hydrate-forming conditions, particularly in porous media; the best approach is perhaps the U.S. Geological Survey gas hydrate and sediment test laboratory instrument (GHASTLI) technique [Winters *et al.*, 2000]. A more convenient technique for making laboratory samples of methane hydrate involves reaction of methane gas with melting granulated water ice [Stern *et al.*, 2000], but this process occurs in nature only over a limited range of conditions. Tetrahydrofuran (THF) hydrate can be reliably synthesized from a stoichiometric solution of the reactants [Pearson *et al.*, 1986], but neither the reactants nor the process reflect natural conditions. Other methods are reviewed by Sloan [1998] and Makogon *et al.* [1998].

[8] Keeping these caveats in mind, laboratory experiments can provide useful insights into natural materials. Pore-space growth habit is most sensitively probed by acoustic measurements. Berge *et al.* [1999], working with CCl₃F hydrate synthetically prepared in sediment, found that the hydrate is not cementing at saturations below 35% and is cementing at higher saturations. Kunerth *et al.* [2001] worked with THF-hydrate and came to the conclusion that it grew with a pore-filling habit.

2.4. Sonic and Seismic Survey Studies

[9] Unlike core recovery or laboratory studies, seismic surveys probe undisturbed natural gas hydrates within the Earth. As noted in the previous section, acoustic properties of hydrate-affected sediments are very sensitive to the growth habit of hydrate. However, the spatial resolution of seismic investigations is poor, and it is difficult to invert seismic information to find material properties in the real heterogeneous Earth. Even more seriously, the hydrate content is usually rather poorly determined and moreover may be heterogeneous over the length scale of the measurement. Despite these uncertainties, sonic and seismic interpreters have attempted to define the pore-space growth habit of hydrate. As recently as a few years ago, it appeared that the cementing growth habits might be common. However, the most recent analyses of acoustic data appear to point toward pore-filling growth habits at Blake Ridge [Jakobsen *et al.*, 2000; Helgerud, 2001], in Alaska [Helgerud, 2001] and in the Mackenzie Delta [Sakai, 2000; Lee and Collett, 2001].

2.5. Transparent Micromodels

[10] Experiments with transparent micromodels have contributed important insights into the nature of hydrate formation in porous media [Tohidi *et al.*, 2001]. Tetrahydrofuran hydrate was formed from a solution of the miscible components, methane hydrate was formed from free gas in water, and carbon dioxide hydrate was formed from dissolved gas in water. In all three cases, formation of hydrate left a thin layer of liquid water wetting the solid surfaces. Methane hydrate first formed at gas-water interfaces, with the gas bubbles slowly converted to hydrate masses as the reaction proceeded.

2.6. Theoretical Models

[11] Theoretical models integrating physical chemistry and geophysics seek to explain histories and morphologies of hydrate-bearing formations. Capillary pressure arguments suggest that hydrate will not form in small pores [Clennell

et al., 1999; *Henry et al.*, 1999; *Clarke et al.*, 1999; *Klauda and Sandler*, 2001]. However, as we shall see later, these arguments are not applicable to coarse-grained sediments and reservoir rocks.

[12] Clearly, the growth habit of methane hydrate in sediments will affect the large-scale structure of hydrate deposits in the Earth. For example, it is recognized that there is an important interaction between the growth habit of hydrate in porous sediment and the resulting hydraulic permeability of the formation [*Nimblett and Ruppel*, 2003]. However, some of the most important inputs into these models are uncertain, and the experimental information needed to resolve the ambiguities is absent.

3. Nuclear Magnetic Resonance Measurements

[13] Despite a great deal of work using a variety of observational, experimental, and theoretical techniques, the growth habit of methane hydrate in porous media is still uncertain. Direct evidence has been scarce and often subject to interpretation. In an effort to better define the nature of hydrate in porous media, we have undertaken a new class of experiments. We created methane hydrate at or near the seafloor, where temperatures and pressures are within the gas hydrate stability zone (GHSZ), in samples of quarried rock. Unlike laboratory experiments, we use an essentially open apparatus to simulate the dynamics of natural systems. Sample properties are then measured by nuclear magnetic resonance (NMR) of hydrogen in fluids. The application of NMR to deep water studies of gas hydrates in rocks and sediments has been described elsewhere [*Kleinberg et al.*, 2003] and is briefly recapitulated here.

3.1. Spin Dynamics

[14] An NMR measurement is made by first aligning magnetic nuclei along a magnetic field B_0 produced by permanent magnets, resulting in a nuclear magnetization M_0 proportional to the number of these nuclei in the affected volume of sample. This alignment, or polarization, is described by an approach to equilibrium that is asymptotic in time t :

$$M(t) = M_0 \left[1 - \exp\left(-\frac{t}{T_1}\right) \right] \quad (1)$$

The time constant T_1 is called the longitudinal relaxation time. Following polarization, the nuclei are irradiated by an antenna which transmits pulses having a carrier frequency $f_0 = (\gamma/2\pi) \cdot B_0$, where γ is the magnetogyric ratio of the nucleus of interest. The constant γ is different for each nuclear species; for 1H , $\gamma/2\pi = 42.58$ MHz/T. These pulses manipulate the orientation of the proton magnetic moments.

[15] Measurements of transverse nuclear magnetic relaxation times, T_2 , have proven to be particularly useful in porous media studies [*Kleinberg*, 1999]. The Carr-Purcell-Meiboom-Gill (CPMG) measurement of transverse relaxation [*Carr and Purcell*, 1954; *Meiboom and Gill*, 1958] consists of a sequence of radio frequency pulses:

$$90^\circ - T_E/2 - (180^\circ - T_E/2 - \text{echo} - T_E/2)_n - W. \quad (2)$$

In this notation, 90° and 180° refer to the angles through which the pulses rotate the nuclear magnetic moments. When irradiated with this pulse sequence, a nuclear spin system will return a series of equally spaced spin echoes, one after each 180° pulse. For the experiments reported here, the echo spacing $T_E = 200$ μ s. The loop in parentheses was repeated 5000 times to acquire a complete record of echo amplitude decay. After the end of each series of echoes the spins repolarized along B_0 during the polarization time W , equal to 8 s for these measurements. The entire sequence was repeated to stack data, echo by echo, with acquisition times generally totaling about 20 min. Measuring the decay of echo amplitudes during the sequence monitors the transverse magnetization relaxation, which in bulk liquids is characterized by a single exponential decay with a time constant T_2 . The zero-time amplitude of the proton NMR signal is M_0 , which is proportional to the hydrogen atom content of the sample.

[16] The sensitivity of the measurement depends on the proton density of the sample and the relaxation times T_1 and T_2 . A substance having a long proton longitudinal relaxation time (T_1) will require a long polarization time to reach its full equilibrium magnetization; if a short polarization time is used, the signal will be diminished according to equation (1), with $t = W$. On the other hand, solids, which generally have very short transverse relaxation times (T_2), will not be detected because complete relaxation occurs before the detection of the first echo at $t = T_E$. Proton NMR, as practiced here, is sensitive primarily to the hydrogen in liquid water. It is partially sensitive to free methane gas and insensitive to methane hydrate.

3.2. Water in Porous Media

[17] Liquid water returns a strong signal, for which the apparatus is calibrated. In the course of pulse sequence (equation (2)) the amplitudes of successive echoes decay. The decay rate is, in the present case, sensitive to the size of the pores in which the water resides and to the density of paramagnetic ions on the grain surfaces [*Kleinberg*, 1999]. The spin echo signal from water in large pores decays more slowly than the signal from water in small pores because the relaxation time of water in a pore depends on the surface-to-volume ratio, $(A/V)_{\text{pore}}$. The echo amplitude from water in a single pore decays exponentially in time, where $t = nT_E$ for the n th echo

$$M(t) = M_0 \exp\left(-\frac{t}{T_2}\right) = M_0 \exp\left[-\left(\rho_2 \left(\frac{A}{V}\right)_{\text{pore}} + \frac{1}{T_{2B}}\right)t\right]. \quad (3)$$

M_0 is the echo amplitude extrapolated to $t = 0$. T_{2B} is the relaxation time of water in bulk, i.e., in the absence of the porous medium. The relaxivity ρ_2 is the constant of proportionality between the pore surface-to-volume ratio and the NMR relaxation rate. The relaxivity depends on the specific combination of mineral grain and pore fluid. For water in typical sands and sandstones it has a value of about 5 μ m/s [*Kleinberg*, 1999], while for the Berea sandstone used here, $\rho_2 = 11$ μ m/s [*Kleinberg et al.*, 2003].

[18] Natural rocks and sediments have broad distributions of pore sizes and the signals from the pores add linearly. Thus the observed spin echo signal is

$$M(t) = \sum_i m_i \exp\left(-\frac{t}{T_{2i}}\right) = \sum_i m_i \exp\left[-\left(\rho_2 \left(\frac{A}{V}\right)_i + \frac{1}{T_{2B}}\right)t\right], \quad (4)$$

where m_i is proportional to the water-filled volume of the i th pore, which has a NMR relaxation time of T_{2i} and a surface-to-volume ratio of $(A/V)_i$. The sum of the coefficients m_i is proportional to the water-filled volume fraction of the sample, the so-called NMR porosity:

$$\sum_i m_i \propto \phi_{\text{NMR}}. \quad (5)$$

[19] Conceptually, the pores are sorted into bins, each of which covers a narrow range of pore sizes and corresponding relaxation times. Equation (4) is a prescription for a signal-processing algorithm which estimates the function $m_i = m(T_{2i})$, commonly called the relaxation time distribution. This function is readily transformed to a pore-size distribution $m(r)$, where r is the pore radius. The transformation depends on the geometrical model adopted for the pores. We adopt the model, generally used in porosimetry, of a network of interconnected tubes, for which $A/V = 2/r$, so

$$r = \frac{2\rho_2}{\frac{1}{T_2} - \frac{1}{T_{2B}}} \approx 2\rho_2 T_2. \quad (6)$$

3.3. Methane Gas

[20] The effect of methane gas on the NMR measurement is somewhat more complicated. It returns a signal proportional to its hydrogen atom density, which at deep water conditions is not negligible. The number density of hydrogen, when normalized by the hydrogen atom density of distilled water at 1 atm (1 atm = 101,325 Pa) and 20°C, is called the hydrogen index, HI. See Table A1 for the hydrogen index of methane gas at Monterey Bay conditions.

[21] The methane signal amplitude is reduced by the lack of complete polarization of the nuclear spins. This reduction is a function of the wait time between pulse sequences, W , and the NMR longitudinal relaxation time, T_1 :

$$P = 1 - \exp\left(-\frac{W}{T_1}\right). \quad (7)$$

Increasing pressure and decreasing temperature both increase T_1 [Gerritsma *et al.*, 1971]. At seafloor conditions, the relaxation time of methane is several seconds, comparable to the wait time used in these experiments, and the polarization P departs significantly from unity (see Table A1). Gas can be distinguished from liquid water by making amplitude measurements at several depths, as discussed in Appendix A.

[22] Methane transverse relaxation is characterized by a very broad distribution of relaxation times induced by the

inhomogeneity of the static magnetic field of the NMR apparatus. Therefore it contributes a broad, low-amplitude background to the distribution function $m(T_2)$ [Flaum, 2000].

3.4. Methane Hydrate

[23] Methane hydrate contains abundant hydrogen, in both its water and methane fractions, but this hydrogen is invisible because our NMR apparatus is not sensitive to hydrogen in solids. Therefore when it is present, hydrate reduces the apparent NMR porosity [Kleinberg *et al.*, 2002, 2003]. It also diminishes the integrated amplitude and changes the shape of the apparent (i.e., water-filled) pore-size distribution. These changes depend on where the hydrate resides within the pore space and on the magnetic coupling between pore water and hydrate.

[24] If hydrate coats grain surfaces, its relaxivity to water, $\rho_2(\text{water-hydrate})$, replaces $\rho_2(\text{water-rock})$ in equation (4). Pore-size information will be retained, but the transformation between T_2 and pore radius is changed. On the other hand, if the hydrate grows in the interior of pores, its surfaces add to the silica grain surfaces, and equation (4) must be generalized to account for the simultaneous influence of two different surfaces.

[25] In order to estimate the relaxivity, laboratory NMR relaxation time measurements have been made at 2°C and 1-atm pressure on liquid-water-saturated THF hydrate powder having a surface area of a few square meters per gram (Straley *et al.*, unpublished data). THF hydrate was employed because it is stable at atmospheric pressure. This allows it to be ground and the surface area measured by standard laboratory techniques. It has been found that $\rho_2(\text{water-hydrate})$ is an order of magnitude smaller than $\rho_2(\text{water-rock})$. We assume that the interaction between water and methane hydrate is similar. Some caution is required here because the structures and molecular motions of methane and THF in their respective hydrates are quite different [Garg *et al.*, 1974; Davidson *et al.*, 1977], and these molecular motions contribute to the strength of the surface relaxivity. We further assume that ρ_2 is insensitive to pressure, as it is for water in sandstone [Chen *et al.*, 1994].

[26] Since it appears likely that the relaxivity of methane hydrate is weak, there would be substantial effects on NMR relaxation if hydrate were to coat pore walls. The T_2 distribution of rock would tend to move to longer times; negligible relaxivity would result in a single relaxation time characteristic of bulk water, $T_{2B} \sim 1.7$ s. If, however, hydrate accumulates in the centers of the pores, its contribution to the relaxation of pore water would be minimal compared to relaxation at the rock surfaces, and the main effect on T_2 would be through the altered microgeometry of liquid water within the pores.

4. Apparatus, Samples, and Method

[27] Deep water experiments were conducted using the remotely operated submersible vehicle ROV *Tiburón*. Power and two-way telemetry are provided by a tether to the mother ship, RV *Western Flyer*. *Tiburón* is equipped with a manipulator arm, gas-handling equipment, video cameras, and other ancillary devices needed to perform a

variety of experiments. It is described in detail elsewhere (MBARI, Marine operations vessels and vehicles, 2003, available at <http://www.mbari.org/dmo/vessels/vessels.htm>).

[28] Nuclear magnetic resonance measurements are not normally performed outside of laboratory or clinical settings. The rigors of seafloor deployment suggested the use of an oilfield wire line NMR tool, the Schlumberger combinable magnetic resonance tool (CMR). The CMR and its integration with the *Tiburion* are described elsewhere [Kleinberg *et al.*, 2003]. The CMR has the unusual capability of making proton nuclear magnetic resonance measurements at 2.2 MHz on compact samples external to its 13-cm-diameter housing [Kleinberg *et al.*, 1992]. The prolate probed volume is approximately 100 cm^3 , centered 2.5 cm from the face of the instrument.

[29] The samples used in this investigation were rods of Berea sandstone, cut from a single quarried block. Laboratory NMR-determined values of porosity ϕ and permeability k (see section 7.3) are listed in Table 1. Samples were transported to the seafloor in acrylic tubes, 76 mm OD, 54 mm ID, and 300 mm long. The interior volume included 92.5% of the NMR-sensitive volume. The tubes were individually machined to minimize dead volume: the resonated volume not within the sample was entirely within the wall of the tube, which contributed no signal. Any signal from bulk seawater inside or outside the sample tubes would have a clear signature at long relaxation time; there was no evidence of this.

[30] While the Berea 3 and Berea 4 samples were transported to ocean depths, 18 moles of methane gas were allowed to bubble through and around the two vertical samples in parallel. This is approximately eight times the quantity of methane required to fully saturate the pore space of the two rocks with hydrate. Gas was introduced at the bottom of each tube and vented at the top. No special precautions were taken to prevent hydrate from forming barriers between gas and water. Gas and water floods were alternated several times as the samples descended at about 30 m/min to and through the gas hydrate stability zone of Monterey Bay. The samples were first taken to 2500-m depth, where NMR measurements were made. The samples were then moved to 1250-m depth, with no addition of gas, for further measurements.

[31] The Berea 5 sample was transported to the seafloor with its own gas supply. Hydrate was formed during the descent using a technique similar to that used for Berea 3 and Berea 4. Eight moles of methane were bubbled through this sample, about seven times as much as required to saturate the rock with hydrate. Unlike the two earlier samples, gas flow through Berea 5 was impeded at about 1400-m depth. NMR measurements were made at 2000 m. The sample was then moved to 1000-m depth, with no addition of gas, for further measurements. A second descent

Table 1. Petrophysical Properties^a

Sandstone	Porosity	T_{2LM} , ^b s	Permeability, darcy
Berea 3	0.229	0.248	0.677
Berea 4	0.238	0.192	0.473
Berea 5	0.229	0.217	0.518

^a1 darcy = $0.987 \times 10^{-12} \text{ m}^2$.

^bFor T_{2LM} definition, see equation (12).

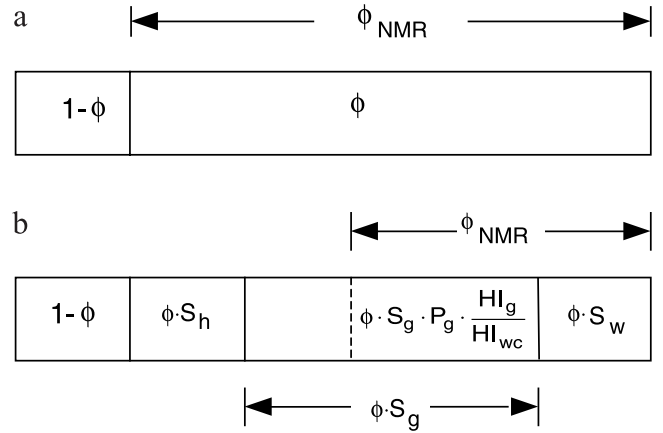


Figure 1. Porosity models for NMR measurement of sandstone. The symbol ϕ represents rock porosity, ϕ_{NMR} is apparent porosity measured by NMR, and S_w , S_g , and S_h are water, gas, and hydrate saturations, respectively. (a) In the laboratory, fully water-saturated. (b) In deep water with water, methane gas, and methane hydrate in the pore space.

to 2000 m with the attempted addition of gas was followed by ascent to 600 m.

5. Measurements and Data Reduction

5.1. Saturations

[32] The fraction of the porosity occupied by hydrate (hydrate saturation, S_h) is determined by measuring the total porosity (calibrated NMR amplitude) at the surface and then making NMR amplitude measurements in the ocean after hydrate has been formed at depth. The porosity models for laboratory and deep water measurements are shown in Figure 1.

[33] CMR amplitude measurements have no detectable zero offset or nonlinearity. Thus a one-point calibration is adequate to fully define the sensitivity to fluid protons across the entire measurement range. The noise spectrum of the apparatus used here is white, so the precision of the measurements is proportional to the square root of the measurement time. Operating in the noise environment of the ROV, it was found that the RMS uncertainty in the amplitude measurement could be reduced to $\delta\phi = 0.01$ (where $\phi = 1$ for bulk water) in measurement times of 10–20 min.

[34] The calibration procedure was simplified from our previous technique [Kleinberg *et al.*, 2003]. An acrylic tube of exactly the same dimensions as the sample tubes was filled with beach water doped with a small quantity of nickel chloride to reduce its relaxation time. A calibration sequence was run in situ on this tube immediately prior to each of the experimental measurements. The ratio of sample to calibration amplitudes is identically equal to the apparent NMR porosity. This procedure eliminated the need to apply temperature, pressure, and sample volume corrections to the data. It also circumvented an apparent Y2K bug in the CMR ENP-0 calibration firmware. The amplitude correction due to varying salinity was uncertain but less than 0.5% and was not applied.

[35] The total porosity ϕ was measured by NMR in the laboratory, each rock sample having been saturated with a

sodium chloride solution that matched the salinity of seawater. Multiple replicate measurements showed the porosity measurement to be consistent to within $\delta\phi = 0.003$ ($\phi = 1$ for bulk water). The NMR-sensitive volume was not exactly at the center of the rock cores, so measurements were made with the rocks oriented in several positions in the sample clip. No variations were noted. The porosity does not change with depth because the external pressure and pore pressure remain equal.

[36] The calibrated subsea NMR measurement is the sum of the signal from the water volume and an attenuated signal from the gas volume, as described in section 3 and illustrated in Figure 1b. With the total porosity known from the laboratory measurement, there are three unknowns to be found, namely the fractions of pore space occupied by water, gas, and hydrate. These saturations are denoted S_w , S_g , and S_h , respectively.

[37] Since the three saturations sum to unity, two measurements are required to characterize the sample. These measurements were made at two depths inside the gas hydrate stability zone, at known temperatures and pressures. It is assumed that decreasing the depth has the following effects: (1) no change of hydrate saturation S_h , (2) no change of the mass of gas in the pore space, (3) expansion of the gas in the pore space according to its equation of state with concomitant increase in S_g , and (4) displacement of water from the pore space with concomitant decrease of S_w . The transfer of methane between liquid and gas phases is negligible because the density of methane dissolved in water is at most a few percent of its density in the gas phase. The gas signal attenuation factors are known and are explicitly incorporated into the system of equations used to solve for the saturations. Data reduction details are presented in Appendix A.

5.2. Relaxation Time Distributions

[38] The data were corrected for differing bulk water relaxation times in the laboratory and in deep water (see equation (4)). Under laboratory conditions (21.5°C) the bulk relaxation times are $T_{1L} = T_{2L} = 3.127$ s. At seafloor conditions (1.9°C), the bulk relaxation times are $T_{1D} = T_{2D} = 1.678$ s. The pressure dependence is negligible. A bulk fluid correction was made to laboratory data by multiplying the echo decays $M(t)$ by the factor

$$\exp\left(-\frac{t}{T_{2D}} + \frac{t}{T_{2L}}\right). \quad (8)$$

Then each term in both the laboratory and deep water multiexponential decays had an apparent parallel decay process with a time constant T_{2D} , corresponding to the bulk relaxation time of water at seafloor conditions. This is important for comparing laboratory and seafloor relaxation time distributions.

[39] The monotonic but nonexponential magnetization decays were fit to equation (4), where $M(t)$ represented the amplitudes of 5000 spin echoes equally spaced in time, and the T_{2i} were 50 preselected time constants, equally spaced on a logarithmic scale between $T_{2\min}$ and $T_{2\max}$. The number of terms in the summation is somewhat arbitrary since the exponentially decaying basis functions are not linearly independent. In fact, there are far less than

Table 2. Hydrate Production

Sample	Depth, m	Saturation, % Pore Volume			Signal Origin, %	
		Hydrate	Methane	Water	Methane	Water
Berea 3	2500	2	13	85	5	95
	1250		25	73	7	93
Berea 4	2500	5	13	82	5	95
	1250		25	70	8	92
Berea 5	2000	25	3	72	1	99
	1000		7	68	2	98
	2000	23	3	74	1	99
	600		10	67	7	93

50 independent pieces of information in a typically noisy decay. Therefore the sets of 50 m_i were found using a regularized nonnegative least squares technique that renders the results smooth and stable in the presence of random noise [Butler *et al.*, 1981]. The degree of smoothing depends on the signal-to-noise ratio of the data, with lower S/N data forcing smoother distributions, i.e., less character is permitted in the result. The function $m_i = m(T_2)$, conventionally called a relaxation time distribution or T_2 distribution, maps nearly linearly to a volumetrically weighted distribution of pore sizes [Gallegos and Smith, 1988]. Porosities were computed by summing the 50 coefficients.

[40] Undiagnosed interference corrupted the early echoes. Therefore the first 300 of 5000 echoes (60 of 1000 ms) were not included in the processing of the measurements; the results reported here are sensitive to water-filled spaces having radii in the range 0.3–30 μm . Corresponding laboratory data were processed the same way to compare with seafloor measurements.

6. Results

6.1. Saturations

[41] Sandstone samples Berea 3 and Berea 4 were alternately flooded with methane and water while descending to 2500-m depth. NMR amplitude measurements at 2500 and 1250 m were compared to determine the hydrate, gas, and water saturations at both depths; see Appendix A for details. The results are summarized in Table 2. In both cases only a small fraction of the pore space was filled with methane hydrate, despite the fact that in both cases methane gas filled 13% of the pore space at 2500 m. At this depth, the temperature was 1.8°C and the pressure was 25 MPa (see Table A1), well within hydrate stability conditions.

[42] The third rock core, Berea 5, was alternately flooded with methane and water while descending to 2000-m depth, transported to 1000 m without further addition of methane, taken back to 2000 m for further flushing with methane, and finally transported to 600 m, which is still within the hydrate stability zone. NMR measurements were made at each depth, and the hydrate, methane gas, and water saturations were determined at each station (see Table 2).

[43] From the first two measurements on Berea 5 it was determined that about 25% of the pore space was filled with hydrate. At 2000 m, methane gas occupied only about 3% of the pore space. Thus conversion to hydrate appears to have been reasonably efficient. However, repeatedly flushing the sample with gas during a second dive to 2000 m

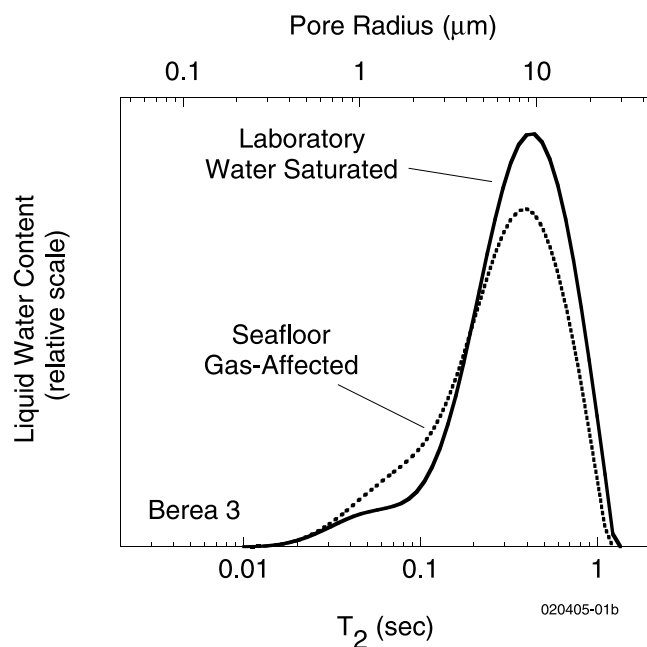


Figure 2. Laboratory relaxation time distribution of water-saturated sandstone (solid curve) and seafloor relaxation time distribution of the same sandstone with 13% methane gas saturation and 2% hydrate saturation (dotted curve). The upper axis is computed using equation (6) with $\rho_2 = 11 \mu\text{m/s}$. The signal from the largest pore spaces (longest T_2) is reduced in the presence of gas, which this measurement does not detect. Additional signal appears at intermediate pore sizes in the presence of gas. This is due to partial occlusion of large pore spaces, increasing the surface-to-volume ratio of the liquid water remaining in these pores.

produced no further hydrate accumulation and, perhaps significantly, no additional methane gas saturation.

6.2. Relaxation Time Distributions

[44] Transverse relaxation time distributions provide unique information about the distribution of water and methane hydrate in the pore space of rock. We have previously published our predictions of how the presence of hydrate should affect the T_2 distribution of water in consolidated rock in two cases: when hydrate occupies the smallest pore spaces (i.e., cementing) and when it occupies the pore bodies (i.e., noncementing) [Kleinberg *et al.*, 2003].

[45] Figure 2 shows the T_2 distributions for Berea 3 fully saturated with water in the laboratory and after flushing with methane while descending to a depth of 2500 m in Monterey Bay. As noted above, volumetric analysis showed that about 2% of the pore space was filled with hydrate, 13% was filled with methane gas, and the remainder was filled with water. Although the methane gas signal contributes to the total NMR amplitude, it is essentially invisible on this plot because it is not sensitive to pore size and is spread out over the entire range of relaxation times [Flaum, 2000]. Thus Berea 3 provides a good example of how pore water redistributes itself in the presence of a significant amount of gas. Compared to the laboratory result, the 2500-m results are depressed at long values of T_2 . This suggests

that gas displaces water from the largest pores, a familiar result. Strong capillary forces associated with the gas-water interface exclude gas from the smallest pore spaces in the rock, and bubbles of gas will tend to reside in the centers of the largest pores.

[46] Figure 2 also suggests, counterintuitively, that the presence of gas enhances the amplitude of signal from the smaller pores, for which $T_2 < 0.2$ s. This effect is widely observed in NMR well logs of natural gas reservoirs and is easily explained. When a nonwetting phase occupies large pores, water generally continues to coat pore walls. The surface-to-volume ratio (A/V) of this pore-lining water is much greater than A/V of water when it completely filled the same pore. Thus the remnant water relaxes at a faster rate (see equation (3)), thereby appearing to add to the smaller-pore population [Kleinberg and Boyd, 1997].

[47] After the first flushing sequence while descending to 2000 m, hydrate and gas occupied 25 and 3%, respectively, of the Berea 5 pore space. The T_2 distribution at this point is compared to the laboratory measurement in Figure 3. Because hydrate is invisible and the methane gas contribution is a broad, low-amplitude background, this figure, like the previous one, is simply reflective of the pore environments of liquid water. When partially filled with hydrate, the signal from the largest pores is suppressed, indicating that hydrate is present in them. The water remaining in the large pores has an enhanced surface-to-volume ratio and therefore appears to add to the population of smaller pores, as in Figure 2. Thus we conclude that hydrate occupies the largest pores in this rock sample. Although this measurement is insensitive to pore spaces smaller than about $0.5 \mu\text{m}$, we believe it unlikely that hydrate formed in the largest and

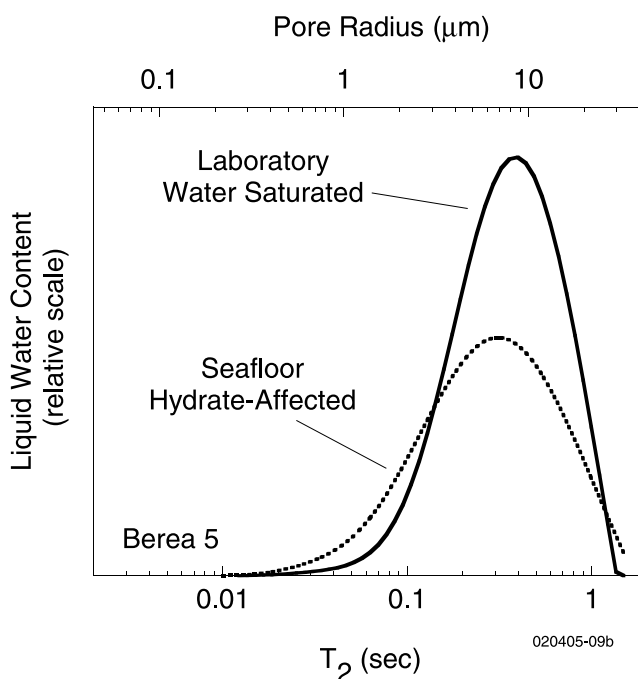


Figure 3. Same as Figure 2, but with 3% methane gas saturation and 25% hydrate saturation.

smallest pores, leaving intermediate-size pores relatively unaffected.

7. Discussion

7.1. Nucleation of Hydrate

[48] The results illustrate the inconsistent nature of hydrate production. Methane was bubbled through the samples while diving, with accompanying pressure changes that might have broken hydrate films protecting gas bubbles from further reaction. Nonetheless, in the four attempts on three samples documented here, a substantial amount of hydrate was produced only once. Similar inconsistencies were found during earlier seafloor experiments. In some cases, methane hydrate formed rapidly in unconsolidated sand and mud [Brewer *et al.*, 1997], while at other times the same procedures produced little or no hydrate in identical materials [Kleinberg *et al.*, 2003, also unpublished data].

[49] The problem of nucleating methane hydrate from a mixture of water and free gas is well documented. The molecular diameter of methane is not well matched to the cage sizes of either structure I or structure II hydrate. Other gases such as xenon or ethane form hydrates more readily [Christiansen and Sloan, 1994]. In the laboratory, induction times for hydrate formation from water and pure methane gas range from a few minutes to more than 24 hours [Skovborg *et al.*, 1993; Yousif, 1994; Natarajan *et al.*, 1994]. Stirring reduces the induction time [Martynets *et al.*, 2002]; analogous natural processes might be found at prolific seafloor gas vents.

[50] Experiments in glass micromodels [Tohidi *et al.*, 2001] showed that THF-hydrate formed rapidly from a concentrated solution. However, methane hydrates formed much more slowly from free gas bubbles in water. Even when cooled 11°C below the thermodynamic transition temperature, 12 hours was required to initiate the formation of hydrate.

[51] Hydrate formation has also been found to be delayed in consolidated rock. Laboratory experiments monitored the generation of methane hydrate from gas in three Berea sandstones cores [Yousif and Sloan, 1991]. In all three, there were long induction times, followed by slow accumulation of hydrate in the pore space. In the most permeable core, the one most similar to the Berea samples used in the present investigation, no hydrate formed in the first hour, and then accumulated slowly over the next 5 hours.

7.2. Growth Habit

[52] The results described in section 6.2 strongly suggest that hydrate, when formed from free gas, occupies the largest pores in consolidated rock. Theories have been proposed that are consistent with this finding, but their employment must respect their limitations. We argue that thermodynamic considerations do not explain the present experimental results.

[53] It is generally accepted that hydrate growth is inhibited in very small pore spaces [Clennell *et al.*, 1999; Henry *et al.*, 1999; Clarke *et al.*, 1999; Klauda and Sandler, 2001]. The basic assumption is that in the presence of hydrate, silica surfaces are liquid-water-wet. The existence of an analogous layer of liquid water between mineral surfaces and water ice is well documented (see section 2.1).

For example, the existence of unfrozen water at pore walls in the presence of ice has been demonstrated by NMR [Overloop and Van Gerven, 1993; Valiullin and Furo, 2002].

[54] From elementary thermodynamics [see, e.g., Clennell *et al.*, 1999] the freezing point T_{fb} in a cylindrical pore of radius r_p is

$$\frac{T_{fb} - T_{fp}}{T_{fb}} = \frac{2\gamma \cos \theta}{\rho \Delta H r_p}, \quad (9)$$

where γ is the surface free energy of the hydrate, θ is the contact angle of the hydrate interface at the pore wall, ρ is the density, ΔH is the specific enthalpy of hydrate dissociation, and T_{fb} is the freezing point of hydrate in bulk in °K.

[55] It is evident from equation (9) that the growth behavior of hydrate depends on its bounding interface. In our experiments, in which the rock was alternately flooded with excess methane gas and excess unsaturated seawater, it is not clear whether the relevant bounding surface is a hydrate-water or hydrate-gas interface. Because of this ambiguity, it is not clear which parameters to use in equation (9). For example, for H₂O at 0°C the surface free energy of the ice-vapor interface is $\gamma_{sv} = 69 \text{ mJ/m}^2$ [Petrenko and Whitworth, 1999], while for the ice-liquid interface it is $\gamma_{sl} = 28 \text{ mJ/m}^2$ [Franks, 1982]. These values may be the same for hydrates [Wilder *et al.*, 2001] or they may be very different when hydrate grows in porous media [Zatsepina and Buffett, 2002].

[56] In previous investigations [Handa and Stupin, 1992; Uchida *et al.*, 1999], experiments were performed on water in capillaries exposed to excess methane gas, so the bounding surfaces were very likely hydrate-gas interfaces. It was found [Uchida *et al.*, 1999]

$$\frac{\Delta T_{fp}}{T_{fp}} = 0.0016 - \frac{0.23 \text{ nm}}{2r_p}. \quad (10)$$

The first term is an unexplained but small offset in the limit of infinite pore radius.

[57] NMR measurements reported here are sensitive to pore radii in the range 0.3–30 μm , for which equation (10) suggests that the freezing point depression is negligible. At seafloor conditions (seawater, 20 MPa), the ambient temperature, 2°C, is well below the hydrate freezing point, approximately 17°C. Thus thermodynamic pore-size control is not a factor in the present experiments.

[58] We believe that methane hydrates form in the largest pore spaces because it is only here that both reactants are present in substantial quantities. Gaseous methane, a nonwetting phase, will be confined to the largest diameter pore spaces. Because of the low solubility of methane in water, hydrate forms primarily at the surfaces of the gas bubbles, which are gradually consumed in place [Kvamme, 2002].

7.3. Hydraulic Permeability

[59] A NMR-permeability equation that has gained broad acceptance in oilfield NMR logging is the Kenyon relationship [Kenyon, 1992; Straley *et al.*, 1994]

$$k = C\phi^4 T_{2LM}^2. \quad (11)$$

T_{2LM} is the logarithmic mean value of the T_2 distribution

$$T_{2LM} = 10 \left[\frac{(1/\phi) \sum_i m(T_{2i}) \log_{10}(T_{2i})}{\sum_i m(T_{2i})} \right]. \quad (12)$$

C is a constant which depends on mineralogy; previous measurements on Berea sandstone showed $C = 4000$ darcy/s² [Kleinberg et al., 2003] (1 darcy = 0.987×10^{-12} m²). T_{2LM} is conceptually related to the pore-space surface-to-volume ratio, A/V , through equation (3), so equation (11) can be written as

$$k \sim \frac{\phi^4}{(A/V)_{\text{pore}}^2} \quad (13)$$

and is thus seen to be related to the Kozeny family of permeability estimates [Scheidegger, 1960]. The constant C in equation (11) is expected to be proportional to the square of the surface relaxivity, ρ_2^2 .

[60] A note of caution is in order. The Kenyon relationship is empirical, based on measurements of several thousand water-saturated sandstone core plugs. Its application to rocks and sediments partially saturated with hydrate must be considered carefully. The effect of hydrate on the porosity term of equation (11) is reasonably simple. With respect to flow, hydrate acts as an addition to the solid grain space. Thus it is sensible to use the NMR-apparent porosity, which excludes the volume of hydrate.

[61] There are larger uncertainties connected with the mineralogy constant C . Since it depends on the relaxivity, ρ_2 , it is specific to each fluid-solid pair. As discussed in section 3.4, we believe ρ_2 for the hydrate-water interface to be an order of magnitude smaller than for the sandstone-water interface. Therefore if hydrate coats the grains, the appropriate value of C is expected to be 100 times smaller than its nominal sandstone value. If, however, hydrate accumulates in the centers of the pores its primary effect is to alter the pore-space geometry.

[62] Using the evidence of the T_2 distributions, we assume that hydrate is located at the centers of pores. We further assume that the Kenyon equation can be used without modification, with $C = 4000$ darcy/s², to predict the hydraulic permeability of hydrate-affected rock and sediment. Then the NMR-determined relative permeability to water, k_{rw} , is

$$k_{rw} = \frac{k(S_w)}{k_0} = S_w^4 \left(\frac{T_{2LM}(S_w)}{T_{2LM}(1.0)} \right)^2, \quad (14)$$

where $k_0 = k(S_w = 1)$ and $k(S_w)$ are the permeabilities to water for water-filled rock and for rock with water saturation S_w , respectively, and $T_{2LM}(S_w)$ and $T_{2LM}(1.0)$ are the logarithmic means of the T_2 distributions at water saturations of S_w and 1.0, respectively.

[63] Berea 5 (2000 m, first descent) has water ($S_w = 0.72$), hydrate ($S_h = 0.25$) and gas ($S_g = 0.03$) in the pore space. Since both gas and hydrate are nonwetting and reside in the largest pore spaces, we assume they block water flow in the same way. This is not quite true, but since the gas saturation is low, we believe that a simple two-component model is a reasonable representation of the hydraulics of Berea 5. For

Table 3. Relative Permeability $S_w = 0.72$

	k_{rw}	Equation
	<i>Experiment</i>	
NMR correlation	0.167	(14)
	<i>Models</i>	
Capillary coating	0.518	(B10)
Pore coating	0.440	(B25)
Pore filling	0.177	(B27)
Capillary filling	0.107	(B14)
LBNL	0.0480	(B29), $m = 0.46$ (B30), $S_r = 0.09$
Tokyo	0.0374	(B28), $N = 10$
Tokyo	0.00724	(B28), $N = 15$

$S_w = 0.72$ and $T_{2LM}(S_w)/T_{2LM}(S_w = 1) = 0.788$, the NMR-estimated relative permeability to water is $k_{rw} = 0.167$.

[64] It is instructive to compare the NMR estimate of relative permeability in the presence of hydrate with theoretical models. Computational details are in Appendix B. Exact calculations show the effect of hydrate growing on the walls, or in the centers, of cylindrical capillary tubes. In other models, Kozeny-like theories of grain packs [Scheidegger, 1960] are developed for pore-filling and pore-coating growth habits. None of these models have adjustable parameters. Table 3 shows that the Berea 5 result is in much better agreement with the pore-filling models than with the pore-coating models. This is consistent with the propositions that hydrate is formed in the centers of pores and that the Kenyon equation is an adequate permeability model for hydrate-affected rock.

[65] We have also examined the results of relative permeability predictions used in some contemporary reservoir simulators. The Tokyo predictions [Masuda et al., 1997] are based on ad hoc adjustments of a capillary tube model in which hydrate coats the pore walls. The LBNL model [Moridis et al., 1998] uses an equation, with no adjustable parameters, derived from studies of shallow terrestrial soils partially saturated with water [Parker et al., 1987]. These models are compared in Table 3. Neither the Tokyo nor LBNL models agree with the Berea 5 result.

[66] These comparisons raise as many questions as they answer. There is a clear need for direct relative permeability measurements on hydrate-affected porous media. It would be very desirable for magnetic resonance measurements such as those reported here to be made on the same samples for the purpose of developing a more refined correlation that can be used to characterize hydraulic properties of natural earth formations in situ.

7.4. Implications for Deposit Accumulation

[67] Gas hydrate deposits accumulate when methane combines with water at appropriate temperature and pressure conditions. It is believed that in some cases methane is dissolved in water and moves into and through the gas hydrate stability zone by diffusion and slow advection [Rempel and Buffett, 1997; Xu and Ruppel, 1999]. Indeed, gas phase methane cannot exist in thermodynamic equilibrium with excess water within the GHSZ.

[68] However, this near-equilibrium process is not the only means by which hydrate can accumulate, and it may not be the most common process. The preponderance of substantial hydrate accumulations appear to be associated

with tectonic features such as fracture or fault systems [Booth *et al.*, 1998] through which dissolved or gaseous methane can move upward rapidly [Clennell *et al.*, 2000b]. This flux may not be in thermodynamic equilibrium with its surroundings. Hydrates are associated with natural gas vents and seeps in the Black Sea [Ivanov *et al.*, 1998], off the Pacific Coast of North America [Spence *et al.*, 2000; Wood *et al.*, 2002], in the Gulf of Mexico [Roberts, 2001; Sassen *et al.*, 2001], and elsewhere. Even the Blake Ridge deposit, situated on a passive margin, is associated with normal faults extending from below the bottom simulating reflector to the seafloor. These faults are believed to constitute efficient conduits for transport of methane [Rowe and Gettrust, 1994; Booth *et al.*, 1998], which may be in the gas phase [Paull *et al.*, 1995; Gorman *et al.*, 2002] and therefore out of thermodynamic equilibrium with surrounding sediments. We believe that our preparation method is a good model for this situation.

[69] In the Earth, efficient transport of free gas in faults can bypass surrounding sediments, but when a fault intersects a layer of coarse sand beneath a permeability barrier, the gas can spread horizontally to produce a hydrate horizon. Fine sediments that do not block water flow may block upward migration of free gas due to capillary pressure effects [Revil *et al.*, 1998; Clennell *et al.*, 2000b]. The formation of hydrate will itself tend to block further flow of fluids [Evrenos *et al.*, 1971; Katoh *et al.*, 2000], especially gas.

[70] Our results are relevant to situations in which water in medium to coarse sediments is exposed to free methane, in which hydrate will fill the largest pore spaces. In consolidated sediments this growth habit will lead to rapid permeability reduction and capillary sealing with respect to free gas. Therefore creation of disseminated hydrate in such systems will be self-limiting. This effect may have been observed in the second attempt to produce hydrate in Berea 5, in which a second attempt to flood the rock with free methane changed neither hydrate nor gas saturations.

[71] In unconsolidated sediments the growth of hydrate in the largest pore bodies permits rearrangement of mineral grains and leaves connected water paths through the sediment. These are the conditions required for the growth of hydrate nodules and lenses. By contrast, if the first appearance of hydrate were to cement the sediment, grain redistribution leading to the formation of massive hydrate bodies would be much less likely. Thus the results of our experiments are consistent with the observed medium-scale structure of some of the most important natural hydrate deposits.

[72] The present results do not bear on hydrate accumulation from low fluxes of dissolved methane; in that case the growth habit and corresponding permeability reduction remain open questions [Nimblett and Ruppel, 2003].

7.5. Implications for Seafloor Stability and Global Climate Change

[73] Release of methane from hydrate deposits has been cited as a driver of global climate change [Kennett *et al.*, 2003]. Decomposition of Arctic hydrate deposits as a result of rising Arctic temperatures may well accelerate global warming [Kvenvolden, 1993], but the role of marine hydrates in global climate change has been less clear. It has been identified as a negative feedback element, reversing global cooling trends upon release of methane during

sea level low stands associated with glaciation [Paull and Ussler, 1991]. More recently, it has been recognized that warming conditions can also lead to a release of marine hydrates [Xu *et al.*, 2001; Vogt and Jung, 2002]. However, it has been uncertain whether methane gas can reach the atmosphere to accelerate warming trends [Kastner, 2001; Matsumoto *et al.*, 2002] or if it is completely oxidized within sediments and the water column, with significant geochemical effects but little if any influence on climate [Dickens, 2001].

[74] Delivery of methane to the atmosphere depends upon both rapid release from sediments and rapid transport through the water column. The possibility of the latter has recently been established by observations of natural gas hydrate rapidly rising through the ocean as intact chunks and decomposing into water and methane gas at or near the sea surface [Suess *et al.*, 2001; Brewer *et al.*, 2002]. Transport of free methane gas to shallow depths is also more efficient than heretofore expected, due to the presence of a hydrate skin which protects gas bubbles until they reach the upper gas hydrate stability horizon [Suess *et al.*, 2001; Rehder *et al.*, 2002].

[75] A catastrophic event is required to release methane or methane hydrate from sediments quickly. Regardless of growth habit, hydrate stiffens sediments in which it exists, and this semiconsolidated mass overlies the highly fluidized and frequently gassy silts and muds at the base of the GHSZ. The setting is reminiscent of avalanche conditions on a snow-covered mountain. Booth *et al.* [1994] have pointed out that slide scars on the U.S. Atlantic margin are strongly correlated with the shallow-water limit of gas hydrate stability; Paull *et al.* [2000] review causative effects. Hydrate decomposition not only reduces the cohesiveness of the sediment body but also creates pore pressure anomalies that further reduce its shear strength [Kayen and Lee, 1991].

[76] If hydrate were to grow preferentially as cement, its contribution to the mechanical strength of the sediment would be retained until its saturation was reduced to a low level. However, if hydrate occupies the centers of pores, as reported here, it will retract from pore walls at the onset of decomposition with associated reduction of strength. Gross motion becomes progressively easier as hydrate shrinks in the pore space.

[77] When hydrate is concentrated in the largest pore bodies the decomposition products will tend to remain trapped in situ, increasing pore pressure, because relative permeability is low until hydrate saturation reaches low values.

[78] Finally, the presence of buoyant hydrate nodules and lenses, a logical consequence of the growth habit observed by NMR, ensures efficient transport of methane into the atmosphere upon seafloor failure.

[79] The concatenation of these effects makes it relatively likely that a small change in hydrate saturation can trigger a submarine slope failure that releases methane into the atmosphere.

8. Conclusion

[80] We have used NMR to determine the pore-scale growth habit of methane hydrate in sandstone. The experi-

Table A1. Physical Properties of Methane and Seawater, November 2001, Monterey Bay, California

Depth, m	T , °C	Pressure, Mpa	Methane Gas							Seawater HI_w	$A = V_m \left(1 - \frac{P_g HI_g}{HI_w} \right)$
			ρ , 0.449168×10^{-4} mol cm ³	T_1 , s	Polarization P_g	Z	V_m , cm ³ /mol	HI_g			
0	15.3	0.100	0.947	0.023	1.00	1.00	23,670	0.00	0.982	23,670	
600	5.45	6.181	68.35	1.47	0.996	0.875	327.9	0.11	0.987	292	
1000	3.89	10.24	122.9	2.67	0.950	0.810	182.3	0.20	0.989	147	
1250	3.24	12.77	160.7	3.50	0.898	0.775	139.5	0.26	0.990	107	
2000	2.06	20.37	262.5	5.75	0.751	0.760	85.38	0.42	0.994	58.3	
2500	1.81	25.43	306.7	6.73	0.696	0.813	73.08	0.50	0.996	47.6	

ments, performed at or near the seafloor in the methane hydrate stability zone, mimic the transport of free methane to coarse-grained sediments far from thermodynamic equilibrium. We find that hydrate forms where the gaseous methane reactant is most abundant: in the largest pore spaces. We suggest that methane hydrate is primarily pore-filling, not grain-cementing, at least in those natural deposits formed by processes analogous to our experimental method. If these results are found to be generally applicable, uncertainties in the interpretation of seismic reflections from hydrate reservoirs will be considerably reduced.

[81] The relative permeabilities of formations to the flow of water and gas also depend crucially on how hydrate forms in the pore space of rock and sediment. Good relative permeability estimates are central to the accuracy of reservoir simulators, which are used to predict how hydrate reservoirs respond to changes in temperature and pressure. These simulators are the principal means by which seafloor and well bore stability, and the economic potential of hydrocarbon reservoirs, are assessed. Relative permeability estimators embedded in contemporary reservoir simulators may need to be revised.

[82] The growth habit clearly influences the mechanism of deposit formation and therefore the gross morphology of hydrate occurrence. Our findings are consistent with field evidence that hydrate grows preferentially in the coarsest available sediments. Moreover, the growth habit we propose is consistent with the creation of nodules and lenses, whereas a cementing habit would tend to suppress these structures.

[83] The mechanical strength of hydrate-affected formations, their relative permeability, and hydrate morphology all contribute to the potential of methane hydrate to participate in global climate change mechanisms. Our results suggest that hydrate formations may be less stable than expected in the presence of changing seafloor temperatures and pressures and that environmentally driven methane release feedback loops may be stronger than heretofore expected.

Appendix A: Data Reduction: Hydrate Saturation

[84] Two corrections are required to convert NMR echo amplitudes to saturations. The first correction accounts for the density of NMR-observable hydrogen atoms in each substance. The hydrogen atom density, normalized by the hydrogen atom density of distilled water at 1 atm pressure and 20°C, is called the hydrogen index. The signal from each substance is proportional to its hydrogen index at measure-

ment depth D divided by the hydrogen index of water at calibration conditions, $HI(D)/HI_{wc}$. For water, the calibration procedure used here ensures that $HI_w(D)/HI_{wc} = 1$ in the laboratory and at all depths. However, $HI_g(D_i)/HI_{wc}$ must be explicitly applied to the gas contribution to the signal. The hydrogen index of seawater and methane as a function of depth is given in Table A1.

[85] The second correction is the polarization correction (equation (7)). W is chosen long enough so that polarization factor for water, P_w , is unity in the laboratory and at all depths. However, the longitudinal relaxation time of methane gas can be long, so the polarization correction must be explicitly applied to it.

[86] The apparent calibrated porosity X at depth D_i is

$$X(D_i) = \phi S_w(D_i) + \phi S_g(D_i) \frac{P_g(D_i) HI_g(D_i)}{HI_{wc}}, \quad (A1)$$

where

- ϕ = laboratory porosity;
 - $S_w(D_i)$ = fraction of pore space occupied by water at measurement depth;
 - $S_g(D_i)$ = fraction of pore space occupied by gas at measurement depth;
 - $HI_g(D_i)$ = hydrogen index of gas at measurement depth;
 - $P_g(D_i)$ = polarization factor for gas at measurement depth;
 - HI_{wc} = water hydrogen index at calibration conditions.
- The polarization correction for methane is

$$P_g = 1 - \exp\left(-\frac{W}{T_1}\right), \quad (A2)$$

where W is the wait time in the pulse sequence. For all measurements $W = 8$ s. For the longitudinal relaxation time T_1 of methane, see Table A1.

[87] At any depth

$$S_w(D_i) + S_g(D_i) + S_h(D_i) = 1, \quad (A3)$$

where $S_h(D_i)$ is the hydrate saturation at measurement depth.

[88] Once the rock has been charged with hydrate, we assume that subsequent depth changes have the following effects: (1) S_h is constant as long as the sample remains in the gas hydrate stability zone and no further gas is introduced. (2) The gas expands according to its equation of state but does not escape from the rock. (3) Water moves in and out of the rock to accommodate gas expansion. The equation of state $PV = nZRT$ has been used for methane gas, with

values of the compressibility factor Z from the work of Amyx *et al.* [1988]; numerical values are furnished in Table A1. Then

$$\frac{S_g(D_1)}{S_g(D_2)} = \frac{V_m(D_1)}{V_m(D_2)}, \quad (\text{A4})$$

where $V_m(D_i)$ is the gas molar volume at the measurement depth. So

$$\frac{X(D_i)}{\phi} = (1 - S_h - S_g(D_i)) + S_g(D_i) \frac{P_g(D_i) \text{HI}_g(D_i)}{\text{HI}_w(D_i)}, \quad (\text{A5})$$

$$\frac{X(D_i)}{\phi} = \left[1 - S_h - S_g(D_i) \left(1 - \frac{P_g(D_i) \text{HI}_g(D_i)}{\text{HI}_w(D_i)} \right) \right], \quad (\text{A6})$$

$$S_g(D_i) = \frac{\left(1 - S_h - \frac{X(D_i)}{\phi} \right)}{\left(1 - \frac{P_g(D_i) \text{HI}_g(D_i)}{\text{HI}_w(D_i)} \right)}. \quad (\text{A7})$$

There are two unknowns in this equation, S_h and $S_g(D_i)$. To eliminate the latter, we use equation (A4)

$$\frac{S_g(D_1)}{S_g(D_2)} = \frac{V_m(D_1)}{V_m(D_2)} = \frac{\left(1 - S_h - \frac{X(D_1)}{\phi} \right) \left(1 - \frac{P_g(D_2) \text{HI}_g(D_2)}{\text{HI}_w(D_2)} \right)}{\left(1 - S_h - \frac{X(D_2)}{\phi} \right) \left(1 - \frac{P_g(D_1) \text{HI}_g(D_1)}{\text{HI}_w(D_1)} \right)}. \quad (\text{A8})$$

To save writing we define

$$A_i \equiv V_m(D_i) \left(1 - \frac{P_g(D_i) \text{HI}_g(D_i)}{\text{HI}_w(D_i)} \right) \quad (\text{A9})$$

and

$$B_{12} \equiv \frac{A_1}{A_2} = \frac{V_m(D_1)}{V_m(D_2)} \frac{\left(1 - \frac{P_g(D_1) \text{HI}_g(D_1)}{\text{HI}_w(D_1)} \right)}{\left(1 - \frac{P_g(D_2) \text{HI}_g(D_2)}{\text{HI}_w(D_2)} \right)}, \quad (\text{A10})$$

$$B_{12} = \frac{\left(1 - S_h - \frac{X(D_1)}{\phi} \right)}{\left(1 - S_h - \frac{X(D_2)}{\phi} \right)}, \quad (\text{A11})$$

$$S_h = 1 - \frac{X(D_1) - B_{12}X(D_2)}{\phi(1 - B_{12})}. \quad (\text{A12})$$

To estimate the hydrate saturation with maximum precision from equation (A12), the difference waveform

$$M(t, D_1) - B_{12}M(t, D_2) \quad (\text{A13})$$

was inverted to obtain the calibrated difference amplitude $X(D_1) - B_{12}X(D_2)$. Then $S_g(D_1)$ is found from equation

(A7) and gas saturation at other depths is found from equation (A4). Water saturation is determined by difference (equation (A3)).

Appendix B: Permeability Models

[89] In the laminar regime relevant to natural porous media, the volumetric rate of fluid flow through a cylindrical channel is proportional to the fourth power of the channel radius. For a channel of elliptical cross section with semiminor axis x and semimajor axis y where $y \gg x$, the flow rate is proportional to x^3y [Lamb, 1945]. Thus flow through porous media is dominated by the continuous flow channel with the largest minimum cross-sectional dimension [Thompson *et al.*, 1987].

[90] The permeability of a porous medium partially saturated with hydrate depends critically on where hydrate forms in the pore space. Consider the limiting case of an infinitesimal film of solid. If this film coats the pore walls, there is an infinitesimal effect on fluid flow. If the film divides the flattened elliptical channel into two ducts, each with small dimension $x/2$, the flow rate will decrease by a factor of four. If the film blocks the cross section, the permeability is reduced to zero. We describe several simple models of permeability reduction and discuss their applicability to our experimental findings.

B1. Parallel Capillary Models

[91] The simplest model of a porous medium consists of a bundle of straight, parallel cylindrical capillaries having inner radius a and length L . The flux of fluid through a unit cross-sectional area containing n such capillaries is [Scheidtger, 1960]

$$q = \frac{n\pi a^4 \Delta p}{8\mu L}, \quad (\text{B1})$$

where μ is the dynamic viscosity (units of mass/(length \times time)) and $\Delta p/L$ is the pressure gradient. The hydraulic permeability k is defined by

$$q = \frac{k \Delta p}{\mu L}, \quad (\text{B2})$$

and the number of capillaries per unit cross-sectional area, n , is related to the porosity ϕ by

$$\phi = n\pi a^2, \quad (\text{B3})$$

so in this model the permeability in the absence of hydrate, k_0 , is

$$k_0 = \frac{\phi a^2}{8}. \quad (\text{B4})$$

B1.1. Hydrate Coats Capillary Walls

[92] If hydrate uniformly coats the walls of each capillary, the radius of the water-filled pore space will be reduced to a_r . Then equation (B1) becomes

$$q = \frac{n\pi a_r^4 \Delta p}{8\mu L}. \quad (\text{B5})$$

Since the number of capillaries per unit cross section remains $n = \phi/\pi a^2$, the permeability to water is reduced to

$$k(S_h) = \frac{\phi a_r^4}{8a^2}. \quad (\text{B6})$$

S_h is hydrate saturation (the volume fraction of pore space occupied by hydrate), and

$$a_r^2 = a^2(1 - S_h), \quad (\text{B7})$$

so

$$k(S_h) = \frac{\phi a^2(1 - S_h)^2}{8}. \quad (\text{B8})$$

[93] The relative permeability to water is defined by

$$k_{\text{rw}} = \frac{k(S_h)}{k_0}, \quad (\text{B9})$$

so for pore-lining hydrate

$$k_{\text{rw}} = (1 - S_h)^2 = S_w^2. \quad (\text{B10})$$

B1.2. Hydrate Occupies Capillary Centers

[94] The simplest permeability model in which hydrate avoids grain surfaces assumes that hydrate forms in the centers of cylindrical pores, leaving an annular flow path for water. The radius of the pore is a , and the radius of the hydrate core is b . In this case, the volume rate of fluid flow in a single tube is [Lamb, 1945]

$$Q = \frac{\pi \Delta p}{8\mu L} \left[a^4 - b^4 - \frac{(a^2 - b^2)^2}{\log\left(\frac{a}{b}\right)} \right]. \quad (\text{B11})$$

The hydrate saturation is

$$S_h = \left(\frac{b}{a}\right)^2. \quad (\text{B12})$$

Following the same steps as above, the permeability of a material composed of a bundle of such capillaries is

$$k(S_h) = \frac{\phi a^2}{8} \left[1 - S_h^2 - \frac{(1 - S_h)^2}{\log\left(\frac{1}{S_h^{0.5}}\right)} \right]. \quad (\text{B13})$$

Then the relative permeability to water is:

$$k_{\text{rw}} = 1 - S_h^2 + \frac{2(1 - S_h)^2}{\log(S_h)} = 1 - (1 - S_w)^2 + \frac{2S_w^2}{\log(1 - S_w)}. \quad (\text{B14})$$

B2. Kozeny Grain Models

[95] Permeability prediction for granular media is considerably more difficult than for simple ducts. No one model is

generally accepted for rock and sediment. The pore spaces are irregular, and flow paths are longer than the straight-line distance L that defines the pressure gradient. A widely used starting point is the Kozeny family of hydraulic permeability equations [Scheidegger, 1960]. There are a number of equivalent forms [Hearst et al., 2000], in which A always refers to the internal surface area of the pore space: (1) expressed in terms of the ratio of the pore surface area to the pore volume:

$$k = \frac{\phi}{\nu\tau(A/V)_{\text{pore}}^2}, \quad (\text{B15})$$

(2) expressed in terms of the ratio of the pore surface area to the overall rock volume:

$$k = \frac{\phi^3}{\nu\tau(A/V)_{\text{rock}}^2}, \quad (\text{B16})$$

(3) expressed in terms of the ratio of pore-surface area to grain volume

$$k = \frac{\phi^3}{\nu\tau(1 - \phi)^2(A/V)_{\text{grain}}^2}, \quad (\text{B17})$$

where ν is a shape factor, which is on the order of unity. Tortuosity is

$$\tau = \left(\frac{L_a}{L}\right)^2, \quad (\text{B18})$$

where L_a is the path length for flow, which is longer than the straight-line distance L associated with the pressure drop Δp . The relationship between the tortuosity τ , the electrical formation factor F , and the porosity ϕ is [Hearst et al., 2000]

$$\tau = F\phi. \quad (\text{B19})$$

[96] Combining equations (B9), (B15), and (B19) and assuming the shape factor ν does not change with hydrate saturation, we have

$$k_{\text{rw}} = \frac{F_0}{F(S_h)} \left(\frac{A_0}{A(S_h)}\right)^2 \left(\frac{V(S_h)}{V_0}\right)^2. \quad (\text{B20})$$

[97] To estimate the Kozeny grain-pack relative permeability, one needs to understand how the electrical formation factor and the surface-to-volume ratio change in the presence of hydrate. Both quantities are model-dependent. Spangenberg [2001] thoroughly discusses the electrical problem for various hydrate growth habits. The relationship between the formation factor in a hydrate-saturated medium, $F(S_h)$, and in a fully water-saturated rock, F_0 , is

$$\frac{F(S_h)}{F_0} = (1 - S_h)^{-n}, \quad (\text{B21})$$

where n is the Archie saturation exponent (see below). Moreover, the pore water volume ratio $V(S_h)/V_0 = 1 - S_h$, so

$$k_{rw} = (1 - S_h)^{n+2} \left(\frac{A_0}{A(S_h)} \right)^2. \quad (\text{B22})$$

B2.1. Hydrate Coats Grains

[98] When hydrate coats the grain surfaces, the surface area of the water-filled pore volume diminishes as the hydrate saturation increases. The cylindrical pore model is the simplest approximation. If the pore radius for $S_h = 0$ is a and the pore radius in the presence of hydrate is a_r , then the surface area ratio is

$$\frac{A_0}{A(S_h)} = \frac{a}{a_r}, \quad (\text{B23})$$

and since $S_h = 1 - (a_r/a)^2$

$$\frac{A_0}{A(S_h)} = (1 - S_h)^{-0.5}, \quad (\text{B24})$$

so equation (B22) becomes

$$k_{rw} = (1 - S_h)^{n+1} = S_w^{n+1}. \quad (\text{B25})$$

[99] For this model, the saturation exponent n equals 1.5 for $0 < S_h < 0.8$ ($1 > S_w > 0.2$) [Spangenberg, 2001]. For $S_h > 0.8$ ($S_w < 0.2$), the saturation exponent diverges, but in this regime the relative permeability to water is already small, and the increase of the saturation exponent has only a minor effect. Thus the relative permeability equation (B25) is similar to equation (B10), despite the fact that the models have different origins.

B2.2. Hydrate Occupies Pore Centers

[100] The pore surface area increases as hydrate grows in the center of the pore. Just before hydrate fills the pore, the surface area is double its original value. In the cylindrical model

$$A(S_h) = A_0(1 + S_h^{0.5}), \quad (\text{B26})$$

hence

$$k_{rw} = \frac{(1 - S_h)^{n+2}}{(1 + S_h^{0.5})^2} = \frac{S_w^{n+2}}{(1 + (1 - S_w)^{0.5})^2}. \quad (\text{B27})$$

Neglecting the effects of capillary pressure, the saturation exponent increases from $n = 0.4$ at $S_h = 0.1$ ($S_w = 0.9$) to unity at $S_h = 1$ ($S_w = 0$), [Spangenberg, 2001].

B3. Other Models

[101] Numerical reservoir simulators predict how hydrate-bearing earth formations respond to temperature, pressure, or chemical perturbations. They account for accumulation and destruction of gas hydrate, and large-scale flows of heat, water, and gas. A number of these simulators are reviewed by Sawyer *et al.* [2000]. The dependence of hydraulic permeability on hydrate saturation is an important

component of the calculations. Here we compare our data to the relative permeability equations used in a few contemporary simulators.

B3.1. University of Tokyo Model

[102] This model [Masuda *et al.*, 1997] takes the capillary tube as a starting point. Hydrate is assumed to line the walls of the capillary, and equation (B10) is derived. In an effort to make the model more realistic, a generalization of equation (B10) is proposed:

$$k_{rw} = (1 - S_h)^N = S_w^N, \quad (\text{B28})$$

where $N = 2$ is the result of the geometrical computation (equation (B10)). It is proposed that N be increased to take into account preferential accumulation of hydrate in pore throats. Masuda *et al.* select $N = 10$ or $N = 15$, but no rationale is given for these specific choices.

B3.2. Lawrence Berkeley National Laboratory Model

[103] The EOSHYDR/TOUGH2 reservoir simulator [Moridis *et al.*, 1998] uses a previously published relative permeability model [van Genuchten, 1980; Parker *et al.*, 1987]:

$$k_{rw} = \bar{S}_w^{1/2} \left[1 - \left(1 - \bar{S}_w^{1/m} \right)^m \right]^2, \quad (\text{B29})$$

with

$$\bar{S}_w = \frac{S_w - S_r}{1 - S_r}, \quad (\text{B30})$$

where S_r is the irreducible water saturation (the fraction of water trapped in the pore spaces of the rock, and therefore immobile at a given pressure gradient). For sandstones such as the Berea rock used here, the irreducible water saturation is equal to the amount of water having NMR $T_2 < 0.033$ s [Straley *et al.*, 1994]. We find $S_r = 0.09$ for the samples used in the present investigation. For sands, silts, and sandstones, $m = 0.46$ [Parker *et al.*, 1987].

[104] **Acknowledgments.** We gratefully acknowledge C. Straley and M. B. Helgerud for discussions and Straley for providing us with data on the relativity of the water-hydrate interface in advance of publication. We also thank C. Ruppel for permission to cite her work prior to publication. J. P. Y. acknowledges support to National Research Laboratory (NRL) from the Office of Naval Research. The success of the experiments depended on the skill and patience of the captain and crew of the *Western Flyer* and the pilots of the *Tiburón*.

References

- Amyx, J. W., D. M. Bass Jr., and R. L. Whiting, *Petroleum Reservoir Engineering: Physical Properties*, McGraw-Hill, New York, 1988.
- Anderson, D. M., Ice nucleation and the substrate-ice interface, *Nature*, 216, 563–566, 1967.
- Berge, L. I., K. A. Jacobsen, and A. Solstad, Measured acoustic wave velocities of R11 (CCl₃F) hydrate samples with and without sand as a function of hydrate concentration, *J. Geophys. Res.*, 104, 15,415–15,424, 1999.
- Booth, J. S., W. J. Winters, and W. P. Dillon, Circumstantial evidence of gas hydrate and slope failure associations on the United States Atlantic continental margin, in *Annals of the New York Academy of Sciences*, vol. 715, *Natural Gas Hydrates*, edited by E. D. Sloan, J. Happel, and M. A. Hnatow, pp. 283–305, N. Y. Acad. of Sci., New York, 1994.
- Booth, J. S., W. J. Winters, W. P. Dillon, M. B. Clennell, and M. M. Rowe, Major occurrences and reservoir concepts of marine clathrate hydrates:

- Implications of field evidence, *Geol. Soc. Spec. Publ.*, 137, 113–127, 1998.
- Brewer, P. G., F. M. Orr Jr., G. Friederich, K. A. Kvenvolden, D. L. Orange, J. McFarlane, and W. Kirkwood, Deep ocean field test of methane hydrate formation from a remotely operated vehicle, *Geology*, 25, 407–410, 1997.
- Brewer, P. G., C. Paull, E. T. Peltzer, W. Ussler, G. Rehder, and G. Friederich, Measurements of the fate of gas hydrates during transit through the ocean water column, *Geophys. Res. Lett.*, 29(22), 2081, doi:10.1029/2002GL014727, 2002.
- Butler, J. P., J. A. Reeds, and S. V. Dawson, Estimating solutions of first kind integral equations with nonnegative constraints and optimal smoothing, *SIAM J. Numer. Anal.*, 18, 381–397, 1981.
- Carr, H. Y., and E. M. Purcell, Effects of diffusion on free precession in nuclear magnetic resonance experiments, *Phys. Rev.*, 94, 630–638, 1954.
- Chen, R., P. E. Stallworth, S. G. Greenbaum, and R. L. Kleinberg, Effects of hydrostatic pressure on proton and deuteron magnetic resonance of water in natural rock and artificial porous media, *J. Magn. Reson., Ser. A*, 110, 77–81, 1994.
- Christiansen, R. L., and E. D. Sloan, Mechanisms and kinetics of hydrate formation, in *Annals of the New York Academy of Sciences*, vol. 715, *Natural Gas Hydrates*, edited by E. D. Sloan, J. Happel, and M. A. Hnatow, pp. 283–305, N. Y. Acad. of Sci., New York, 1994.
- Churaev, N. V., S. A. Bardasov, and V. D. Sobolev, On the non-freezing water interlayers between ice and a silica surface, *Coll. Surf.*, A79, 11–24, 1993.
- Clarke, M. A., M. Pooladi-Darvish, and P. R. Bishnoi, A method to predict equilibrium conditions of gas hydrate formation in porous media, *Ind. Eng. Chem. Res.*, 38, 2485–2490, 1999.
- Clenell, M. B., M. Hovland, J. S. Booth, P. Henry, and W. J. Winters, Formation of natural gas hydrates in marine sediments: 1. Conceptual model of gas hydrate growth conditioned by host sediment properties, *J. Geophys. Res.*, 104, 22,985–23,003, 1999.
- Clenell, M. B., P. Henry, M. Hovland, J. S. Booth, W. J. Winters, and M. Thomas, Formation of natural gas hydrates in marine sediments, in *Annals of the New York Academy of Sciences*, vol. 912, *Gas Hydrates, Challenges for the Future*, edited by G. D. Holder and P. R. Bishnoi, pp. 887–896, N. Y. Acad. of Sci., New York, 2000a.
- Clenell, M. B., A. Judd, and M. Hovland, Movement and accumulation of methane in marine sediments: Relation to gas hydrate systems, in *Natural Gas Hydrate in Oceanic and Permafrost Environments*, edited by M. D. Max, pp. 105–122, Kluwer Acad., Norwell, Mass., 2000b.
- Dash, J. G., H. Fu, and J. S. Wettlaufer, The premelting of ice and its environmental consequences, *Rep. Prog. Phys.*, 58, 115–167, 1995.
- Davidson, D. W., S. K. Garg, S. R. Gough, R. E. Hawkins, and J. A. Ripmeester, Characterization of natural gas hydrates by nuclear magnetic resonance and dielectric relaxation, *Can. J. Chem.*, 55, 3641–3650, 1977.
- Dickens, G. R., Modeling the global carbon cycle with a gas hydrate capacitor: Significance for the latest Paleocene thermal maximum, in *Natural Gas Hydrates: Occurrence, Distribution and Detection*, *Geophys. Monogr. Ser.*, vol. 124, edited by C. K. Paull and W. P. Dillon, pp. 19–38, AGU, Washington, D. C., 2001.
- Dvorkin, J., M. B. Helgerud, W. F. Waite, S. H. Kirby, and A. Nur, Introduction to physical properties and elasticity models, in *Natural Gas Hydrate in Oceanic and Permafrost Environments*, edited by M. D. Max, pp. 245–260, Kluwer Acad., Norwell, Mass., 2000.
- Evrenos, A. I., J. Heathman, and J. Ralstin, Impermeation of porous media by forming hydrates in situ, *J. Pet. Technol.*, 23, 1059–1066, 1971.
- Flaum, C., Nuclear magnetic resonance well logging to determine gas-filled porosity and oil-filled porosity of earth formations without a constant static magnetic field gradient, Patent 6,097,184, U.S. Patent and Trademark Off., Washington, D. C., 2000.
- Franks, F., The properties of aqueous solutions at subzero temperatures, in *Water: A Comprehensive Treatment*, vol. 7, edited by F. Franks, pp. 234–236, Plenum, New York, 1982.
- Gallegos, D. P., and D. M. Smith, A NMR technique for the analysis of pore structure: Determination of continuous pore size distributions, *J. Colloid Interface Sci.*, 122, 143–153, 1988.
- Garg, S. K., D. W. Davidson, and J. A. Ripmeester, NMR behavior of clathrate hydrate of tetrahydrofuran, I, Proton measurements, *J. Magn. Reson.*, 15, 295–309, 1974.
- Gerritsma, C. J., P. H. Oosting, and N. J. Trappeniers, Proton spin-lattice relaxation and self diffusion in methanes, II, Experimental results for proton spin-lattice relaxation times, *Physica*, 51, 381–394, 1971.
- Ginsburg, G., V. Soloviev, T. Matveeva, and I. Andreeva, Sediment grain size control on gas hydrate presence, sites 994, 995, and 997, *Proc. Ocean Drill. Program Sci. Results*, 164, 237–245, 2000.
- Gorman, A. R., W. S. Holbrook, M. J. Hombach, and K. L. Hackwith, Migration of methane gas through the hydrate stability zone in a low-flux hydrate province, *Geology*, 30, 327–330, 2002.
- Graber, K. K., E. Pollard, B. Jonasson, and E. Schulte, Overview of Ocean Drilling Program engineering tools and hardware, *Tech. Note 31*, Ocean Drill. Program, College Station, Tex., 2002.
- Handa, Y. P., and D. Stupin, Thermodynamic properties and dissociation characteristics of methane and propane hydrates in 70 Å radius silica gel pores, *J. Phys. Chem.*, 96, 8599–8603, 1992.
- Handa, Y. P., M. Zakrzewski, and C. Fairbridge, Effect of restricted geometries on the surface and thermodynamic properties of ice, *J. Phys. Chem.*, 96, 8594–8599, 1992.
- Hearst, J. R., P. H. Nelson, and F. L. Paillet, *Well Logging for Physical Properties*, chap. 15, McGraw-Hill, New York, 2000.
- Helgerud, M. B., Wave speeds in gas hydrate and sediments containing gas hydrate: A laboratory and modeling study, Ph.D. dissertation, Stanford Univ., Stanford, Calif., 2001.
- Helgerud, M. B., J. Dvorkin, A. Nur, A. Sakai, and T. Collett, Elastic wave velocity in marine sediments with gas hydrates: Effective medium modeling, *Geophys. Res. Lett.*, 26, 2021–2024, 1999.
- Henry, P., M. Thomas, and M. B. Clennell, Formation of natural gas hydrates in marine sediments: 2. Thermodynamic calculations of stability conditions in porous sediments, *J. Geophys. Res.*, 104, 23,005–23,022, 1999.
- Ivanov, M. K., A. F. Limonov, and J. M. Woodside, Extensive deep fluid flux through the sea floor on the Crimean continental margin (Black Sea), *Geol. Soc. Spec. Publ.*, 137, pp. 195–213, 1998.
- Jakobsen, M., J. A. Hudson, T. A. Minshull, and S. C. Singh, Elastic properties of hydrate-bearing sediments using effective medium theory, *J. Geophys. Res.*, 105, 561–577, 2000.
- Kastner, M., Gas hydrates in convergent margins: Formation, occurrence, geochemistry, and global significance, in *Natural Gas Hydrates: Occurrence, Distribution and Detection*, *Geophys. Monogr. Ser.*, vol. 124, edited by C. K. Paull and W. P. Dillon, pp. 67–86, AGU, Washington, D. C., 2001.
- Katoh, A., K. Nakayama, K. Baba, and T. Uchida, Model simulation for generation and migration of methane hydrate, *Energy Explor. Exploit.*, 18, 401–422, 2000.
- Kayen, R. E., and H. J. Lee, Pleistocene slope instability of gas hydrate-laden sediment on the Beaufort Sea margin, *Mar. Geotechnol.*, 10, 125–141, 1991.
- Kennett, J. P., K. G. Cannariato, I. L. Hendy, and R. J. Behl, *Methane Hydrates in Quaternary Climate Change: The Clathrate Gun Hypothesis*, *Spec. Publ.*, vol. 54, AGU, Washington, D. C., 2003.
- Kenyon, W. E., Nuclear magnetic resonance as a petrophysical measurement, *Nucl. Geophys.*, 6, 153–171, 1992.
- Klauda, J. B., and S. I. Sandler, Modeling gas hydrate phase equilibria in laboratory and natural porous media, *Ind. Eng. Chem. Res.*, 40, 4197–4208, 2001.
- Kleinberg, R. L., Nuclear magnetic resonance, in *Experimental Methods in the Physical Sciences*, vol. 35, *Methods in the Physics of Porous Media*, edited by P.-Z. Wong, chap. 9., Academic, San Diego, Calif., 1999.
- Kleinberg, R. L., and A. Boyd, Tapered cutoffs for magnetic resonance bound water volume, paper presented at the Annual Technical Conference, paper 38737, Soc. of Petrol. Eng., San Antonio, Tex., Oct. 1997.
- Kleinberg, R. L., A. Sezginer, D. D. Griffin, and M. Fukuhara, Novel NMR apparatus for investigating an external sample, *J. Magn. Reson.*, 97, 466–485, 1992.
- Kleinberg, R. L., C. Flaum, C. Straley, P. G. Brewer, G. Malby, E. Peltzer, G. Friederich, and J. P. Yesinowski, Proton nuclear magnetic resonance observation of methane hydrate formation in rock samples in an ROV-controlled seafloor laboratory, paper presented at the Fourth International Conference on Gas Hydrates, Yokohama, Japan, 19–23 May 2002.
- Kleinberg, R. L., C. Flaum, C. Straley, P. G. Brewer, G. E. Malby, E. T. Peltzer III, G. Friederich, and J. P. Yesinowski, Seafloor nuclear magnetic resonance assay of methane hydrate in sediment and rock, *J. Geophys. Res.*, 108(B3), 2137, doi:10.1029/2001JB000919, 2003.
- Kunert, D. C., D. M. Weinberg, J. W. Rector, C. L. Scott, and J. T. Johnson, Acoustic laboratory measurements during the formation of a THF-hydrate in unconsolidated porous media, *J. Seismic Explor.*, 9, 337–354, 2001.
- Kvamme, B., Initiation and growth of hydrate, paper presented at the Fourth International Conference on Gas Hydrates, Yokohama, Japan, 19–23 May 2002.
- Kvenvolden, K. A., Gas hydrates: Geological perspective and global change, *Rev. Geophys.*, 31, 173–187, 1993.
- Kvenvolden, K. A., L. A. Barnard, and D. H. Cameron, Pressure core barrel: Applications to the study of gas hydrates, Deep Sea Drilling

- Project Site 533, leg 76, *Proc. Ocean Drill. Program Initial Rep.*, 76, 367–375, 1983.
- Lamb, H., *Hydrodynamics*, pp. 331–332, Dover, Mineola, N. Y., 1945.
- Lee, M. W., and T. S. Collett, Elastic properties of gas hydrate-bearing sediments, *Geophysics*, 66, 763–771, 2001.
- Makogon, Y. F., T. Y. Makogon, and S. A. Holditch, Several aspects of the kinetics and morphology of gas hydrates, paper presented at the International Symposium on Methane Hydrates: Resources in the Near Future?, Jpn. Natl. Oil Corp., Chiba City, Japan, 20–22 Oct. 1998.
- Martynets, V. G., I. S. Afanas'ev, P. P. Bezverkhi, N. V. Kuskova, and E. V. Matizen, Equilibrium and kinetic properties of methane hydrate, *Theor. Found. Chem. Eng.*, 36, 495–499, 2002.
- Masuda, Y., S. Naganawa, S. Ando, and K. Sato, Numerical calculation of gas production performance from reservoirs containing natural gas hydrates, paper presented at the Annual Technical Conference, paper 38291, Soc. of Petrol. Eng., San Antonio, Tex., Oct. 1997.
- Matsumoto, R., Comparison of marine and permafrost gas hydrates: Examples from Nankai Trough and Mackenzie Delta, paper presented at the Fourth International Conference on Gas Hydrates, Yokohama, Japan, 19–23 May 2002.
- Matsumoto, R., M. H. M. Gharai, and Y. Kakuwa, Was the late Devonian mass extinction caused by massive dissociation of gas hydrate?, paper presented at the Fourth International Conference on Gas Hydrates, Yokohama, Japan, 19–23 May 2002.
- Meiboom, S., and D. Gill, Modified spin echo method for measuring nuclear relaxation times, *Rev. Sci. Instrum.*, 29, 688–691, 1958.
- Moridis, G., J. Apps, K. Pruess, and L. Myer, EOSHYDR: A TOUGH2 module for CH₄-hydrate release and flow in the subsurface, *Rep. LBNL-42386*, Lawrence Berkeley Natl. Lab., Berkeley, Calif., 1998.
- Natarajan, V., P. R. Bishnoi, and N. Kalogerakis, Induction phenomena in gas hydrate nucleation, *Chem. Eng. Sci.*, 49, 2075–2087, 1994.
- Nimblett, J., and C. Ruppel, Permeability evolution during the formation of gas hydrates in marine sediments, *J. Geophys. Res.*, 108(B9), 2420, doi:10.1029/2001JB001650, 2003.
- Overloop, K., and L. Van Gerven, Freezing phenomena in adsorbed water as studied by NMR, *J. Magn. Reson., Ser. A*, 101, 179–187, 1993.
- Parker, J. C., R. J. Lenhard, and T. Kuppusamy, A parametric model for constitutive properties governing multiphase flow in porous media, *Water Resour. Res.*, 23, 614–618, 1987.
- Paull, C. K., and W. Ussler III, Is the extent of glaciation limited by marine gas hydrates?, *Geophys. Res. Lett.*, 18, 432–434, 1991.
- Paull, C. K., W. Ussler III, W. S. Borowski, and F. N. Spiess, Methane-rich plumes on the Carolina continental rise: Associations with gas hydrates, *Geology*, 23, 89–92, 1995.
- Paull, C. K., W. Ussler III, and W. P. Dillon, Potential role of gas hydrate decomposition in generating submarine slope failures, in *Natural Gas Hydrate in Oceanic and Permafrost Environments*, edited by M. D. Max, pp. 149–156, Kluwer Acad., Norwell, Mass., 2000.
- Pearson, C., J. Murphy, and R. Hermes, Acoustic and resistivity measurements on rock samples containing tetrahydrofuran hydrates: Laboratory analogues to natural gas hydrate deposits, *J. Geophys. Res.*, 91, 14,132–14,138, 1986.
- Petrenko, V. F., and R. W. Whitworth, *Physics of Ice*, Oxford Univ. Press, New York, 1999.
- Rehder, G., P. W. Brewer, E. T. Peltzer, and G. Friederich, Enhanced lifetime of methane bubble streams within the deep ocean, *Geophys. Res. Lett.*, 29(15), 1731, doi:10.1029/2001GL013966, 2002.
- Rempel, A. W., and B. A. Buffett, Formation and accumulation of gas hydrate in porous media, *J. Geophys. Res.*, 102, 10,151–10,164, 1997.
- Revil, A., L. M. Cathles III, J. D. Shosa, P. A. Pezard, and F. D. deLarouziere, Capillary sealing in sedimentary basins: A clear field example, *Geophys. Res. Lett.*, 25, 389–392, 1998.
- Roberts, H. H., Fluid and gas expulsion on the northern Gulf of Mexico continental slope: Mud-prone to mineral-prone responses, in *Natural Gas Hydrates: Occurrence, Distribution and Detection*, *Geophys. Monogr. Ser.*, vol. 124, edited by C. K. Paull and W. P. Dillon, pp. 145–161, AGU, Washington, D. C., 2001.
- Rowe, M. M., and J. F. Gettrust, Methane hydrate content of Blake Outer Ridge sediments, in *International Conference on Natural Gas Hydrates*, *Annals of the New York Academy of Sciences*, vol. 715, edited by E. D. Sloan, J. Happel, and M. A. Hnatow, pp. 492–494, N. Y. Acad. of Sci., New York, 1994.
- Sakai, A., Can we estimate the amount of gas hydrates by seismic methods?, in *Gas Hydrates: Challenges for the Future*, *Annals of the New York Academy of Sciences*, vol. 912, edited by G. D. Holder and P. R. Bishnoi, pp. 374–391, N. Y. Acad. of Sci., New York, 2000.
- Sassen, R., S. L. Losh, L. Cathles III, H. H. Roberts, J. K. Whelan, A. V. Milkov, S. T. Sweet, and D. A. DeFreitas, Massive vein-filling gas hydrate: Relation to ongoing gas migration from the deep subsurface in the Gulf of Mexico, *Mar. Pet. Geol.*, 18, 551–560, 2001.
- Sawyer, W. K., C. M. Boyer II, J. H. Frantz Jr., and A. B. Yost II, Comparative assessment of natural gas hydrate production models, paper presented at the Annual Technical Conference, paper 62513, Soc. of Petrol. Eng., Dallas, Tex., 1–4 Oct. 2000.
- Scheidegger, A. E., *The Physics of Flow Through Porous Media*, Macmillan, Old Tappan, N. J., 1960.
- Shipboard Scientific Party, Leg 204 preliminary report, *Prelim. Rep. 104*, Ocean Drill. Prog. College Station, Tex., 2002.
- Skovborg, P., H. J. Ng, P. Rasmussen, and U. Mohn, Measurement of induction times for the formation of methane and ethane gas hydrates, *Chem. Eng. Sci.*, 48, 445–453, 1993.
- Sloan, E. D., *Clathrate Hydrates of Natural Gases*, Marcel Dekker, New York, 1998.
- Spangenberg, E., Modeling of the influence of gas hydrate content on the electrical properties of porous sediments, *J. Geophys. Res.*, 106, 6535–6548, 2001.
- Spence, G. D., R. D. Hyndman, N. R. Chapman, M. Riedel, N. Edwards, and J. Yuan, Cascadia Margin, northeast Pacific Ocean: Hydrate distribution from geophysical investigations, in *Natural Gas Hydrate in Oceanic and Permafrost Environments*, edited by M. D. Max, pp. 183–198, Kluwer Acad., Norwell, Mass., 2000.
- Stern, L. A., S. H. Kirby, W. B. Durham, S. Circone, and W. F. Waite, Laboratory synthesis of pure methane hydrate suitable for measurement of physical properties and decomposition behavior, in *Natural Gas Hydrate in Oceanic and Permafrost Environments*, edited by M. D. Max, pp. 323–348, Kluwer Acad., Norwell, Mass., 2000.
- Straley, C., D. Rossini, H. Vinegar, P. Tutunjian, and C. Morriss, Core analysis by low field NMR, paper presented at the 1994 International Symposium, paper SCA-9404, Soc. of Core Anal., Stavanger, Norway, 12–14 Sept. 1994.
- Suess, E., et al., Sea floor methane hydrates at Hydrate Ridge, Cascadia Margin, in *Natural Gas Hydrates: Occurrence, Distribution and Detection*, *Geophys. Monogr. Ser.*, vol. 124, edited by C. K. Paull and W. P. Dillon, pp. 87–98, AGU, Washington, D. C., 2001.
- Thompson, A. H., A. J. Katz, and C. E. Krohn, The microgeometry and transport properties of sedimentary rock, *Adv. Phys.*, 36, 625–694, 1987.
- Tohidi, B., R. Anderson, M. B. Clennell, R. W. Burgass, and A. B. Biderkab, Visual observation of gas hydrate formation and dissociation in synthetic porous media by means of glass micromodels, *Geology*, 29, 867–870, 2001.
- Uchida, T., T. Ebinuma, and T. Ishizaki, Dissociation condition measurements of methane hydrate in confined small pores of porous glass, *J. Phys. Chem. B*, 103, 3659–3662, 1999.
- Valiullin, R., and I. Furo, The morphology of coexisting liquid and frozen phases in porous materials as revealed by exchange of nuclear spin magnetization followed by ¹H nuclear magnetic resonance, *J. Chem. Phys.*, 117, 2307–2316, 2002.
- van Genuchten, M. T., A closed form equation for predicting the hydraulic conductivity of unsaturated soils, *Soil Sci. Soc. Am. J.*, 44, 892–898, 1980.
- Vogt, P. R., and W.-Y. Jung, Holocene mass wasting on upper non-Polar continental slopes: Due to post-glacial ocean warming and hydrate dissociation?, *Geophys. Res. Lett.*, 29(9), 1341, doi:10.1029/2001GL013488, 2002.
- Wilder, J. W., K. Seshadri, and D. H. Smith, Modeling hydrate formation in media with broad pore size distributions, *Langmuir*, 17, 6729–6735, 2001.
- Winters, W. J., S. R. Dallimore, T. S. Collett, T. J. Katsube, K. A. Jenner, R. E. Cranston, J. F. Wright, F. M. Dixon, and T. Uchida, Physical properties of sediments from the JAPEX/JNOC/GSC Mallik 2L-38 gas hydrate research well, *Geol. Surv. Can. Bull.*, 544, 95–100, 1999.
- Winters, W. J., W. P. Dillon, I. A. Pecher, and D. H. Mason, GHASTLI—Determining physical properties of sediment containing natural and laboratory-formed gas hydrate, in *Natural Gas Hydrate in Oceanic and Permafrost Environments*, edited by M. D. Max, pp. 311–322, Kluwer Acad., Norwell, Mass., 2000.
- Wood, W. T., J. F. Gettrust, N. R. Chapman, G. D. Spence, and R. D. Hyndman, Decreased stability of methane hydrates in marine sediments owing to phase-boundary roughness, *Nature*, 420, 656–660, 2002.

- Xu, W., and C. Ruppel, Predicting the occurrence, distribution, and evolution of methane gas hydrate in porous marine sediments, *J. Geophys. Res.*, *104*, 5081–5095, 1999.
- Xu, W., R. P. Lowell, and E. T. Peltzer, Effect of seafloor temperature and pressure variations on methane flux from a gas hydrate layer: Comparison between current and late Paleocene climate conditions, *J. Geophys. Res.*, *106*, 26,413–26,423, 2001.
- Yousif, M. H., The kinetics of hydrate formation, paper presented at the Annual Technical Conference, paper 28479, Soc. of Petrol. Eng., New Orleans, La., 25–28 Sept. 1994.
- Yousif, M. H., and E. D. Sloan, Experimental investigation of hydrate formation and dissociation in consolidated porous media, *SPE Reservoir Eng.*, *6*, 452–458, 1991.
- Zatsepina, O. Y., and B. A. Buffett, Nucleation of CO₂ hydrate in a porous medium, *Fluid Phase Equilibria*, *200*, 263–275, 2002.
-
- P. G. Brewer, G. E. Malby, and E. T. Peltzer, Monterey Bay Aquarium Research Institute, 7700 Sandholdt Road, Moss Landing, CA 95039-9644, USA. (brpe@mbari.org; gem@mbari.org; etp@mbari.org)
- C. Flaum, D. D. Griffin, and R. L. Kleinberg, Schlumberger-Doll Research, Old Quarry Road, Ridgefield, CT 06877, USA. (cflaum@ridgefield.oilfield.slb.com; dgriffin@ridgefield.oilfield.slb.com; kleinberg@slb.com)
- J. P. Yesinowski, Naval Research Laboratory, Washington, DC 20375, USA. (yesinowski@nrl.navy.mil)